Granular Matter (2025) 27:65
https://doi.org/10.1007/s10035-025-01535-6

RESEARCH

Soil fabric of coarse-grained soils sedimented under water and its relation to relative density and excess pore water pressure

Božana Baćić[1] · **Ivo Herle**[1] · **Martin Oppermann**[2]

Received: 14 February 2025 / Accepted: 10 May 2025

Abstract

The soil fabric varies significantly depending on the deposition process that forms the grain skeleton. Each deposition method produces a specific type of soil fabric, which can be linked to a particular soil density. When represented as relative density, determined using limit densities from standard index tests, a wide range of relative densities can be observed for different sands produced by the same deposition method. The influence of this variation in relative density, resulting from a single deposition method, on the development of the excess pore water pressure (PWP) should be further investigated. A fast testing of the excess PWP accumulation in sandy soils during undrained cyclic shearing can be easily performed using the newly developed PWP Tester. In the PWP Tester, specimens are prepared through sedimentation in water, which yields a comparable fabric in different sands but significantly different relative densities. Despite these relative density differences, the rate of the excess PWP evolution during undrained shearing is remarkably similar among different sands. This indicates that relative density should not be regarded as a primary factor influencing the development of the excess PWP and that the soil fabric plays equal or even a greater role.

Keywords Relative density · Sand fabric · Excess PWP · Water sedimentation · Cyclic shear · PWP Tester

1 Introduction

The discrete nature of granular soils significantly influences their mechanical behaviour, which depends strongly on the effective stress, relative density, etc., but also on their fabric, which is created either through natural processes or artificially at construction sites (e.g. open-pit mines) or in laboratories. The arrangement of soil grains within the skeleton, usually denoted as fabric [1, 2], is mostly described by the spatial orientation of grains and of contact normals at grain contacts. The orientations of the voids between the grains are used for the fabric characterisation in a less extent [3].

In order to obtain different soil fabric in the laboratory, different specimen preparation methods are used. Widely used are dry funnel and water pluviation as well as moist tamping. Sand specimens prepared through dry funnel and water pluviation possess an anisotropic fabric, with grains aligned mostly horizontally [4–9]. According to [10], the fabrics of natural alluvial soils and water pluviated soils in a laboratory are similar. On the contrary, in moist tamped specimens prepared according to the procedure described in [11], the contact normals are predominantly oriented in the vertical direction, and to an even greater extent than in pluviated specimens [12, 13]. Although these fabrics are highly anisotropic, the standard description of soil relies on scalar variables, such as density.

Soils can change volume, and thus density, during shear deformation. Under drained conditions, where water can escape from the pores between the grains without generating excess pore water pressure, volume change (compaction or expansion) depends on several factors. Dense soils tend to dilate, increasing in volume, while loose soils contract, reducing in volume.

✉ Božana Baćić
bozana.bacic@tu-dresden.de

Ivo Herle
ivo.herle@tu-dresden.de

Martin Oppermann
martin.oppermann@tu-dresden.de

[1] Institute of Geotechnical Engineering, TU Dresden, 01062 Dresden, Germany

[2] Electronics Packaging Lab, TU Dresden, 01062 Dresden, Germany

Under undrained conditions, the flow of pore water is not possible and the soil volume remains constant during the shear deformation. Thus, the external monotonic or cyclic loading can lead to an accumulation of the excess pore water pressure (PWP). Consequently, in case of the positive excess PWP the effective stress decreases, which may finally result in a complete loss of shear strength and stiffness. It is often said that the soil ’liquefies’, which is why the accumulation of the positive excess PWP is commonly associated with the phenomenon of soil liquefaction [14].

The role of the stress-dependent soil density in assessing the excess PWP evolution is undisputable. Many authors confirm an increase in the resistance to the excess PWP accumulation with growing relative density [15–22]. However, it is also clear that the soil state and its mechanical response cannot be fully understood by considering only the relative density. For example, under the same testing conditions (relative density, stress level, loading magnitude), the evolution of the excess PWP occurs more rapidly in dry pluviated specimens than in moist tamped specimens [12].

Under the same deposition conditions, such as sedimentation in air or water, a similar fabric can be observed in soils with different granulometric properties. However, the deposition densities, such as the minimum dry densities ($\rho_{d,\min}$), will differ due to these granulometric differences. As a result, comparing the excess PWP for different sands at the same relative density can be misleading if the initial soil state was created using a different method than the one used to determine the reference (limit) values of dry density. In spite of this, a widely used "simplified procedure" [23], based on empirical correlations of liquefaction resistance and soil relative density, has become a standard practice for evaluating liquefaction potential (excess PWP accumulation) in situ. Thus, it is reasonable to question the suitability of relative density as a crucial parameter for the estimation of the excess PWP accumulation during soil shearing.

The primary objective of this study is to evaluate the influence of the soil fabric on the evolution of the excess PWP during cyclic shearing under undrained conditions, focusing on the limitations of a relative density based prediction of the excess PWP accumulation. To address this question, a novel experimental setup called the *PWP Tester* has been developed [24, 25]. The testing procedure enables a rapid and reproducible measurement of the excess PWP evolution in coarse-grained soils. The initial fabric of the tested soils is created through water sedimentation, which makes the method representative of field conditions for many sands. The measured build-up of the excess PWP during cyclic shearing under undrained conditions allows for the determination of the parameters characterising this evolution.

2 PWP Tester

The installed specimen ($D/H = 50$ mm/110 mm) in the PWP Tester (see Fig. 1) resembles a cylindrical triaxial specimen enclosed in a rubber membrane. To achieve a full saturation, prior to the installation, sand is mixed with demineralised water and de-aired under vacuum. This de-aired sand-water mixture is installed using a funnel into the rubber membrane supported by a split mould. By pulling the funnel filled with the de-aired sand-water mixture upwards, the mixture flows out of the funnel and fills the supported membrane (see also Sect. 3.1). After sealing the specimen with the top cap and connecting it to a steel rod, which can oscillate horizontally, the sand is consolidated by applying the suction u_0 to the specimen bottom. Considering that the relative air pressure surrounding the specimen represents the total pressure and equals to 0 kPa, the initial effective stress p'_0 in the specimen is increased by the suction value.

After the consolidation is finished and the split mould is dismounted, the suction valve is closed and the top cap is cyclically moved in horizontal direction with a constant displacement amplitude and frequency. This kind of specimen loading is very similar to the simple shear mode and results in an increase of the excess PWP Δu, which is measured at the specimen bottom. Additionally, the relative air pressure (total stress) surrounding the specimen is measured. The

Fig. 1 A sketch of the PWP Tester

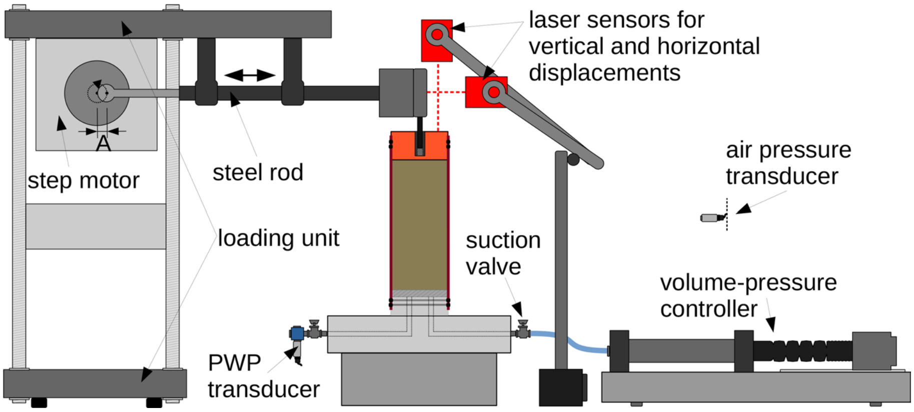

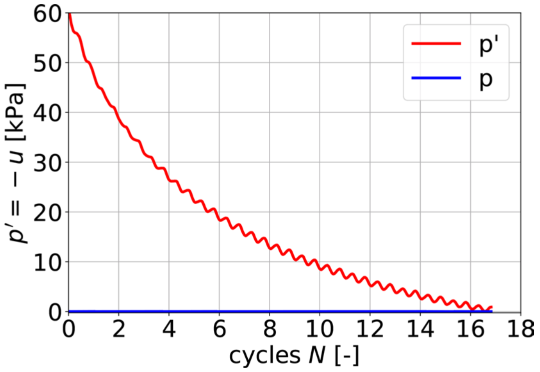

Fig. 2 Evolution of the PWP u, the mean effective stress p' and the mean total stress p with loading cycles N during cyclic shearing in the PWP Tester

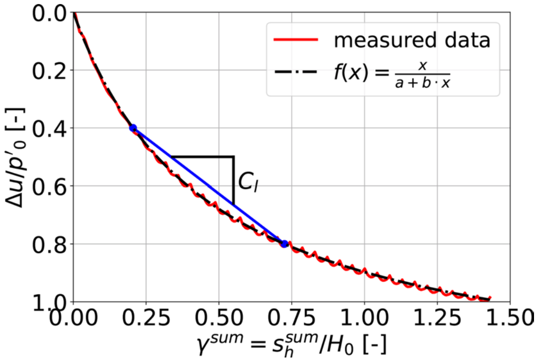

Fig. 3 Determination of the parameter C_l characterising the evolution of the excess PWP with the accumulated shear strain γ^{sum} during cyclic loading

change of the effective stress within the specimen is isotropic and results from the initially applied suction reduced by the excess PWP:

$$\Delta p' = p - \Delta u \quad \rightarrow \quad \Delta p' = -\Delta u \quad \text{since} \quad p = 0. \tag{1}$$

A typical evolution of the PWP u (and thus the effective stress p') as well as the total stress p in the PWP Tester is shown in Fig. 2. Within a single loading cycle, fluctuations in both negative and positive PWP can be observed. After each cycle, the effective stress decreases due to a cumulative permanent increase in the excess PWP. The duration of a single test, including specimen preparation, is approximately 30 min. More details on the PWP Tester and the test performance can be found elsewhere [24–26].

The accumulated displacement of the top cap (measured contactless with a laser distance sensor) in one cycle is $s_h^{sum} = 4 \cdot A$, with A being the amplitude of the horizontal displacement (see Fig. 1). Accordingly, s_h^{sum} in N-cycles corresponds to $s_h^{sum} = 4 \cdot A \cdot N$. Using s_h^{sum}, the accumulated shear strain $\gamma^{sum} = s_h^{sum}/H_0$ can be defined (H_0 corresponds to the initial height of the specimen). Thus, γ^{sum} is increasing during cyclic shearing and corresponds qualitatively to the development of the loading cycles.

In order to characterise the evolution of the excess PWP, a dimensionless parameter C_l, that quantifies an average rate of the generated excess PWP, is introduced. To determine C_l, the evolution of the normalised excess PWP $\Delta u/p'_0$ with the accumulated shear strain γ^{sum} is approximated with a hyperbolic function $f(x) = x/(a + b \cdot x)$(Fig. 3). In this way, the fluctuations of the excess PWP are disregarded in the determination of C_l. In the $\gamma^{sum} - \Delta u/p'_0$ diagram, C_l represents a slope of the secant line to $f(x)$.

The determination of C_l follows from 40 to 80 % of the excess PWP build-up:

$$C_l = \frac{\Delta u/p'_0}{\Delta \gamma^{sum}} = \frac{(\Delta u_{0.8} - \Delta u_{0.4})/p'_0}{\gamma^{sum}_{0.8} - \gamma^{sum}_{0.4}} = \frac{0.4}{\gamma^{sum}_{0.8} - \gamma^{sum}_{0.4}}, \tag{2}$$

see also Fig. 3. The initial cycles are excluded in the determination of C_l to eliminate the influence of the installation effects, while the final stage is disregarded due to the strong heterogeneity of the liquefied specimen. Comparison of C_l for different sands or states does not change significantly when considering secant lines in different ranges [27].

The C_l-parameter represents a state variable, since it depends on the relative density, consolidation pressure, loading displacement, grain and contact orientations in the soil structure, etc. A sand with a higher C_l is more prone to the generation of the excess PWP than a sand with a lower C_l when prepared and tested under the same conditions.

3 Relative density of sands after sedimentation under water

3.1 Experimental testing

The sand specimen created by water sedimentation has the minimum density related to this deposition method. Depending on the granulometric properties (grain shape, uniformity coefficient, mean grain diameter, fines content), it is reasonable to expect that the deposition densities (and thus the relative densities, when considering the limiting dry densities from standard index tests) after the water sedimentation of different sands will be different.

To check the above statement, 41 different materials (see Fig. 4 and Table 3), including mixtures of glass beads and crushed sand, were sedimented under water, analogously to the specimen installation in the PWP Tester, and their dry densities were determined. A simple experimental setup used for this purpose consists out of a metal cylinder, a long-mouth funnel, two long threded rods and a cylinder-extension (see Fig. 5 left).

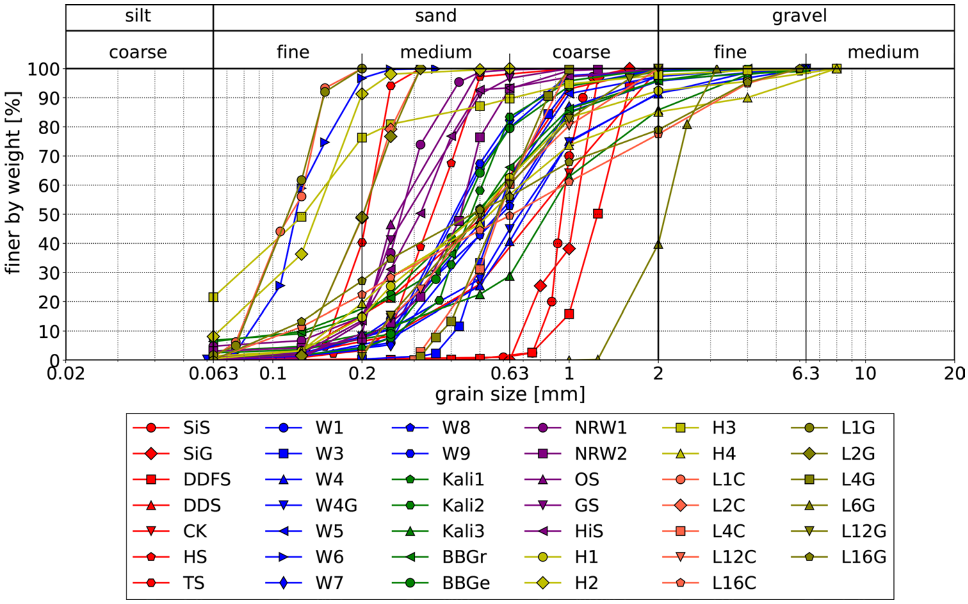

Fig. 4 Grain size distribution curves of the materials sedimented under water

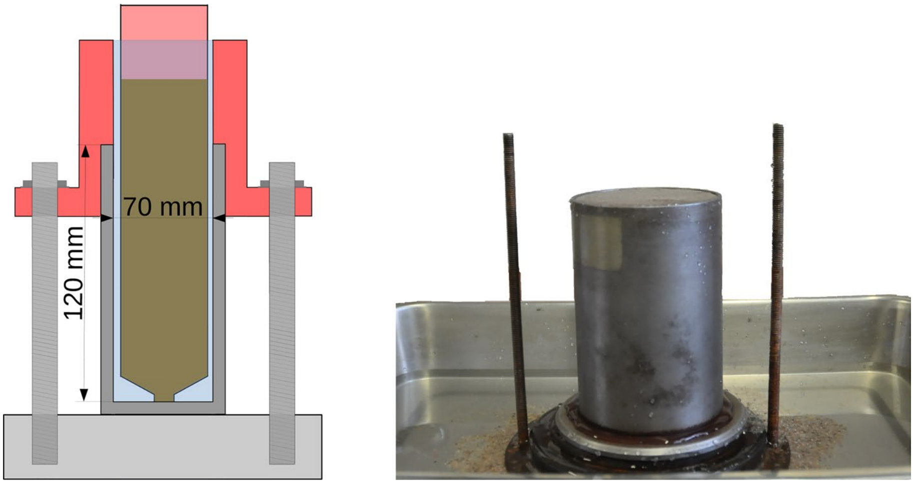

Fig. 5 A sketch of an experimental setup for sand sedimentation under water (left) and an image of the sand-water mixture in the cylinder at the end of the test (right)

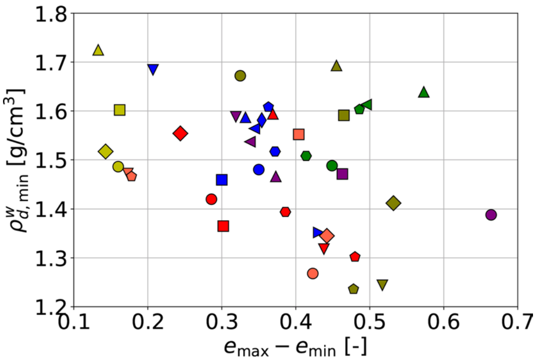

Fig. 6 Dependence between the void ratio range $e_{\max} - e_{\min}$ and the minimum dry density $\rho^w_{d,\min}$ for the tested materials after their sedimentation under water

Upon pouring the sand-water mixture into the long-mouth funnel, the water levels inside and outside of the funnel are the same and remain constant throughout the test, ensuring no hydraulic gradient during the deposition. By slowly pulling the funnel upwards, the mixture flows out of the funnel and fills the cylinder. After removing the water and the mixture above the cylinder as well as the unnecessary installation components (Fig. 5 right), the mixture in the cylinder is oven-dried, and the dry mass m_d of the sand is determined.

Considering the volume V of the cylinder ($D = 70$ mm and $H = 120$ mm) and the dry mass of the sand m_d, the minimum dry density $\rho^w_{d,\min}$ of the tested materials after their sedimentation under water is calculated and plotted in dependence of $e_{\max} - e_{\min}$ in Fig. 6. Here, $e_{\max}$ and $e_{\min}$ are the limiting void ratios corresponding to minimum and maximum dry densities, $\rho_{d,\min}$ and $\rho_{d,\max}$, respectively, which are obtained from the standard index tests [28].

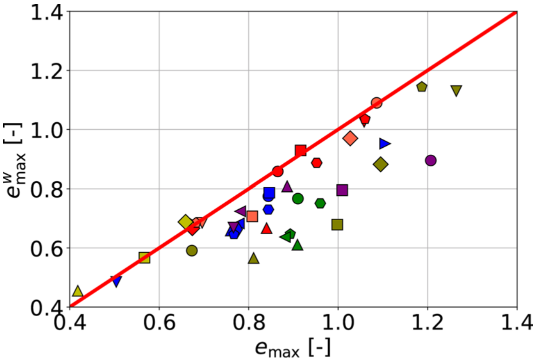

Fig. 7 Dependence between the maximum void ratio $e_{\max}$ and the maximum void ratio after sedimentation under water $e^w_{\max}$ for the tested materials

A slightly decreasing trend with a large $\rho^w_{d,\min}$ band can be observed. Most of the determined dry densities lie in a range between 1.4 and 1.7 g/cm^3, while the densities of more angular and coarse materials (salmon coloured markers) lie below 1.35 g/cm^3.

As shown in Fig. 7, the dependence between the maximum void ratio $e_{\max}$ and the maximum void ratio after sedimentation under water $e^w_{\max}$ reveals that for most materials the void ratio after the sedimentation under water $e^w_{\max}$ is (partly significantly) lower than the void ratio created by dry funnel pluviation (standard $e_{\max}$).

3.2 Parameter I_w

Considering the $\rho^w_{d,\min}$ as well as $\rho_{d,\min}$ and $\rho_{d,\max}$, a soil parameter I_w quantifying the relative density of soil after sedimentation under water is introduced:

$$I_w = \frac{\rho_{d,\max} \cdot (\rho^w_{d,\min} - \rho_{d,\min})}{\rho^w_{d,\min} \cdot (\rho_{d,\max} - \rho_{d,\min})} = \frac{e_{\max} - e^w_{\max}}{e_{\max} - e_{\min}}, \tag{3}$$

where $e^w_{\max}$ is the maximum void ratio corresponding to $\rho^w_{d,\min}$. Figure 8 left illustrates an increasing trend in which I_w rises with $e_{\max} - e_{\min}$. Here, the colours and symbols chosen for different materials correspond to those from Fig. 4. Additionally, the tested materials exhibit distinct groupings based on their granulometric properties (Fig. 8 right).

The results indicate that the glass bead mixtures exhibit negative to very low I_w values. These low I_w values can be attributed to the narrow void ratio range, despite having a similar $\rho^w_{d,\min}$ compared to other materials. Sands with fines content $FC > 1$ % tend to achieve higher relative densities ($I_w > 0.3$) after their water sedimentation compared to materials without fines.

For angular and crushed sands with an $e_{\max} - e_{\min}$ range between 0.38 and 0.52, significant differences in I_w are observed compared to the materials with $FC > 1$ %, with much lower I_w values obtained for angular sands. As highlighted by Cubrinovski and Ishihara [29], the void ratio range reflects all granulometric properties of sands, including C_U, d_{50}, FC and grain shape, which makes it difficult to isolate the effect of a single granulometric property using $e_{\max} - e_{\min}$. This is particularly important for FC and grain shape (or grain angularity), as these properties have opposite effects on the sand compressive behaviour. Obviously, it is possible to distinguish these two material groups based on their I_w, as it strongly differs for sands with certain FC and angular grains while their $e_{\max} - e_{\min}$ range is almost the same.

4 Excess PWP build-up in different sands

4.1 Materials and testing conditions

In order to check the accumulation of the excess PWP, 13 different materials (including 12 different natural sands and one mixture of glass beads) were prepared through sedimentation under water and subsequently tested using the PWP Tester. Grain size distribution curves[1] of these materials are presented in Fig. 9. Most of the tested natural sands have narrow grain size distribution curves, with mean grain sizes from fine to coarse sand, while sands W4, H1 and H4 are characterised by broader grain size distributions. The

Fig. 8 Dependence between the void ratio range $e_{\max} - e_{\min}$ and the parameter I_w for the tested materials (left) and the dependence between the void ratio range $e_{\max} - e_{\min}$ and the parameter I_w represented for material groups with similar granulometric properties (right)

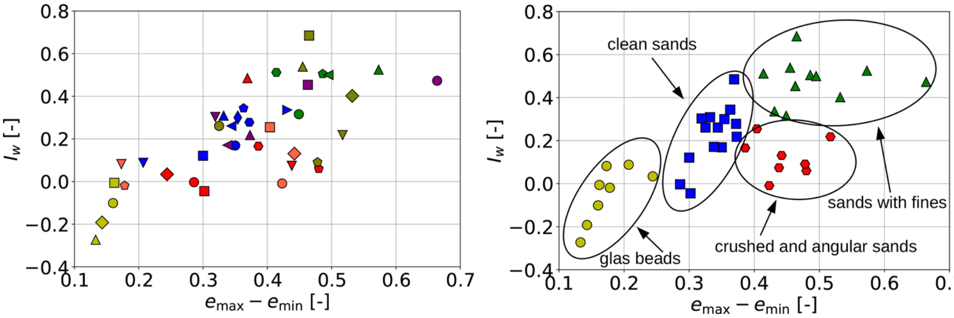

---

[1] Grains with a diameter larger than 5 mm were removed prior to the specimen installation in the PWP Tester.

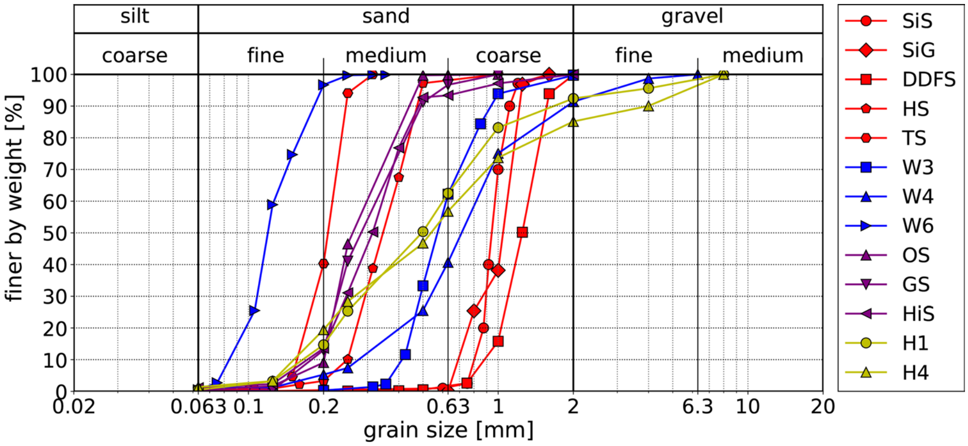

Fig. 9 Grain size distribution curves of the materials tested in the PWP Tester

Table 1 Testing conditions in the PWP Tester

p'_0 [kPa]	A [mm]	f [Hz]	t_m [mm]	H [mm]	D [mm]
60	2.4	1	0.5	110	50

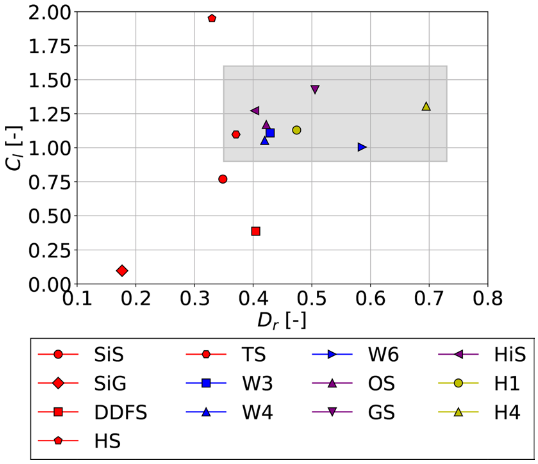

Fig. 10 Dependence between the relative density D_r and the rate of the excess PWP build-up C_l for 13 different materials

glass beads mixture SiG has a grain size distribution that closely resembles that of the SiS sand. All materials have $FC \leq 1\,\%$.

The testing conditions in the PWP Tester for this experimental study can be taken from Table 1. Here, t_m stands for the membrane thickness.

The loading amplitude, frequency and consolidation pressure were selected based on preliminary experimental validation, ensuring a complete reduction in effective stresses within 10 to 20 cycles. This criterion was essential for consistency with the accompanying cyclic undrained triaxial tests (ongoing study), where the same consolidation pressure is used and the cyclic resistance ratio (CRR) is determined as cyclic stress ratio (CSR) at $N = 10$ cycles.

4.2 Results

The rates of the excess PWP accumulation C_l in the PWP Tester (see Sect. 2) related to the relative densities D_r

$$D_r = \frac{\rho_{d,\max} \cdot (\rho_d - \rho_{d,\min})}{\rho_d \cdot (\rho_{d,\max} - \rho_{d,\min})} = \frac{e_{\max} - e}{e_{\max} - e_{\min}} \tag{4}$$

for the considered 13 materials installed by the sedimentation under water are presented in Fig. 10. There are significant differences regarding the relative densities, ranging from loose ($D_r \approx 0.2$) to dense ($D_r \approx 0.7$) state, although the specimen preparation method was the same for all materials. As discussed in Sect. 3.1, these variations of D_r reflect the differences in the granulometric properties of these materials.

In spite of the large differences in D_r, the C_l values of the most materials range between $C_l = 1.0$ and $C_l = 1.5$. Considering the definition of C_l and the dependence between γ^{sum} and N (see Sect. 2), the number of cycles corresponding to the variation of C_l from 1.0 to 1.5 lies between 3 and 8. A few C_l values outside of this range can be noticed. Lower C_l values in case of the most uniform and coarse SiS and DDFS sands can probably be attributed to the membrane penetration effects. Furthermore, the C_l parameter of the coarse glass beads mixture SiG is remarkably low, which also questions the usual hypothesis that round and relatively smooth particles exhibit a lower resistance to the excess PWP accumulation. Another exception is the medium HS sand (also widely known as Hostun sand) having $C_l \approx 2.0$, which makes this sand the most susceptible to the excess PWP build-up of all tested materials. This can probably be attributed to the elongated Hostun sand grains, which create a fabric with a low resistance to the horizontal shearing (see also Sect. 5.2).

It becomes obvious from Fig. 10 that the (conventional) relative density is not a suitable parameter for the characterisation of the soil susceptibility to generate the excess

PWP. It can be assumed that the same deposition method using water sedimentation created a similar soil fabric in all tested sands. Therefore, it seems that the similar soil fabric, induced by the same specimen preparation method, has at least the same or even a stronger impact on the excess PWP accumulation than a standard relative density.

As already stated, the method to prepare specimens in the PWP Tester differs from the one used in standard index tests for the determination of the limit densities ($\rho_{d,\min}$ and $\rho_{d,\max}$) with the corresponding limit void ratios ($e_{\max}$ and $e_{\min}$). Therefore, the relative density D_r(see Eq. 4) includes different types of soil fabric and, thus, does not realistically capture the soil state controlling the current soil response. An alternative definition of the relative density considering the same soil fabric created by the same deposition method used for the specimen preparation and the determination of the soil minimum dry density would be a more appropriate soil state descriptor.

The minimum dry density of soil after sedimentation $\rho^w_{d,\min}$, introduced in Sect. 3.2, is obtained through soil sedimentation under water, which produces the same soil fabric as the one formed in the PWP Tester. Thus, the modified relative density D^w_r, determined from

$$D^w_r = \frac{\rho_{d,\max} \cdot (\rho_d - \rho^w_{d,\min})}{\rho_d \cdot (\rho_{d,\max} - \rho^w_{d,\min})} = \frac{e^w_{\max} - e}{e^w_{\max} - e_{\min}}, \tag{5}$$

where, ρ_d and e are the dry soil density and the void ratio after consolidation and before shearing in the PWP Tester, provides a description of the soil (relative) density that is related to only one particular soil fabric of e and $e^w_{\max}$. This makes it more suitable for describing the soil state when analysing the build-up of excess PWP in different soils.

The modified relative density concept can be extended to soils deposited through different methods. It is necessary to use a consistent method for the reference dry density tests and the actual specimen preparation. Successful integration of this approach in seismic liquefaction assessment or geotechnical engineering design requires an understanding of the in situ soil deposition process. By replicating the deposition method and determining the minimum dry density according to this procedure, the modified relative density can be obtained, thereby achieving a more accurate and fabric-related representation of the in situ soil state.

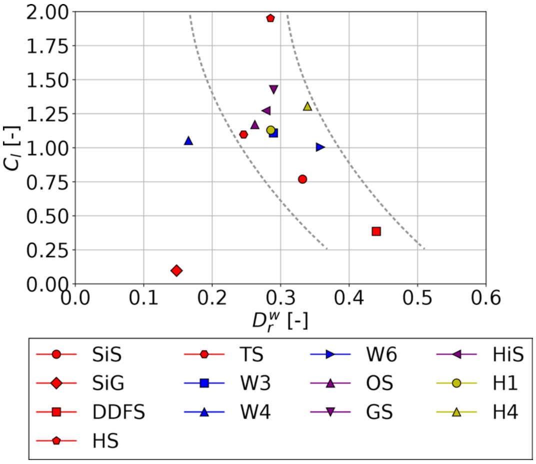

Fig. 11 Dependence between the modified relative density D^w_r and the rate of the excess PWP build-up C_l for 13 different materials

It is important to understand the difference between the parameters I_w and D^w_r. The parameter I_w describes the state of the soil related to the newly defined loosest state after sedimentation under water. The parameter D^w_r represents the soil state corresponding to the current void ratio in the PWP Tester, which is linked to the new limiting maximum void ratio $e^w_{\max}$, obtained through soil sedimentation under water. Also, note that $D^w_r = 0$ holds for all points in Fig. 8.

The dependence between D^w_r and C_l for all materials tested in the PWP Tester (Fig. 11) shows a narrower distribution of D^w_r than D_r(cf. Fig. 10) where the most relative densities correspond to loose state and lie between 0.2 and 0.4. Also, with the exception of glass beads SiG and sand W4, a band can be observed where C_l decreases as D^w_r increases. This confirms the increasing resistance to the excess PWP accumulation with rising modified relative density D^w_r.

One might ask why the D^w_r values are around $D^w_r \approx 0.3$ rather than $D^w_r = 0$, given that the specimen preparation method in the PWP Tester is identical to the one used for determining $\rho^w_{d,\min}$. This difference occurs because the specimens in the PWP Tester are enclosed with a top cap and subjected to a consolidation pressure of 60 kPa, which leads to additional densification of the material.

5 Fabric

To characterise the fabric of materials after their deposition under water and to interpret the results obtained from the PWP Tester, μCT scans (μCT device "nanotom s" by Phoenix|X-ray/Waygate Technologies) were performed for three different materials and the fabric was extracted from these images. The analysed materials include the sands SiS and W3 as well as the glass bead mixture SiG. The large chamber of the μCT scanner enabled the installation of the volume-pressure controller within the chamber during μCT image acquisition, see Fig. 12. This setup ensured that the consolidation pressure of 40 kPa in the specimen ($D/H \approx$ 20 mm/40 mm) remained constant, thereby preventing any grain movement due to potential water evaporation caused by elevated temperatures in the μCT chamber.

Fig. 12 A sand specimen and a volume-pressure controller inside of the μCT chamber

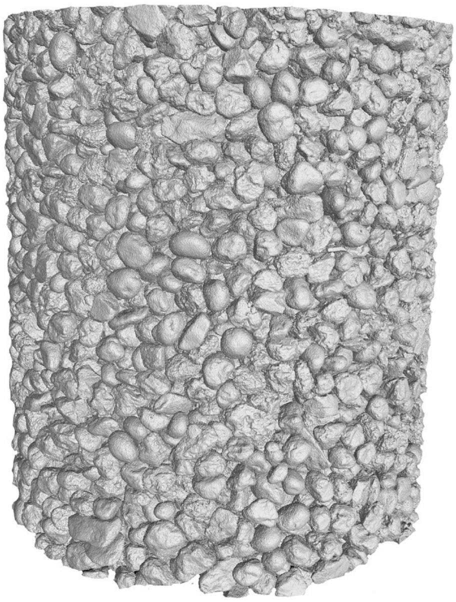

Fig. 13 The 3D rendering of the scanned part of the SiS sand specimen ($D/H \approx$ 20 mm/20 mm)

A single radiograph was captured every 1/4°, resulting in a total of 1440 radiographs, which were subsequently reconstructed into a single 3D μCT image using the software "phoenix_datosx_2_rec". The visualisation of the results was done with "VGSTUDIO MAX 3.3" by Volume Graphics GmbH. The acquisition of one μCT image lasted approximately 2 h. To obtain high-resolution radiographs, achieved by reducing the distance between the X-ray tube and the specimen, only the central part of the specimen ($\approx$ 20 mm) was scanned (Fig. 13). The μCT images in the case of SiS sand and glass beads mixture SiG have a voxel size of 12.5 μm, while the voxel size for the sand W3 is 10.6 μm.

5.1 Image analysis and fabric descriptors

The image analysis was conducted using the open-source software *spam* [30]. For fabric quantification, a benchmark strategy for the experimental measurement of contact fabric, developed by Wiebicke et al. [31], was employed. The computational part of the image analysis and fabric evaluation was performed at the Centre for Information Services and High Performance Computing (ZIH) at the TU Dresden.

To extract the contact fabric from each μCT scan, the images are initially binarized using a global threshold. Subsequently, segmentation is performed via a topological watershed algorithm and a local threshold is applied to improve the contact detection. For a more precise characterisation of the contact plane, a power watershed method, specifically the random walker algorithm, is employed at each contact. This approach enables the determination of the contact plane with a sub-pixel precision. Finally, the contact orientation, defined by the orientation of the contact normal, is computed using principal component analysis (PCA).

Using the contact orientations of the entire specimen, a second order fabric tensor **N**:

$$\mathrm{N} = \frac{1}{N} \sum_{i \in N} \mathrm{o}^i \otimes \mathrm{o}^i, \tag{6}$$

with N being the number of orientations and **o** being one individual orientation, can be built. Furthermore, the contact fabric is described by two scalar variables: the coordination number CN and the contact fabric anisotropy a. The coordination number represents the average number of contacts per grain and can be calculated as

$$CN = 2 \cdot \frac{N_c}{N_p}, \tag{7}$$

with N_c being the number of overall contacts in a grain assembly, and N_p the total number of particles. The contact fabric anisotropy a is calculated from the deviatoric part of the fabric tensor D:

$$a = \sqrt{\frac{3}{2} \mathrm{D} : \mathrm{D}}, \tag{8}$$

where

$$\mathrm{D} = \frac{15}{2} \left(\mathrm{N} - \frac{1}{3} \mathrm{I} \right), \tag{9}$$

with N being the second order fabric tensor and I being the identity tensor.

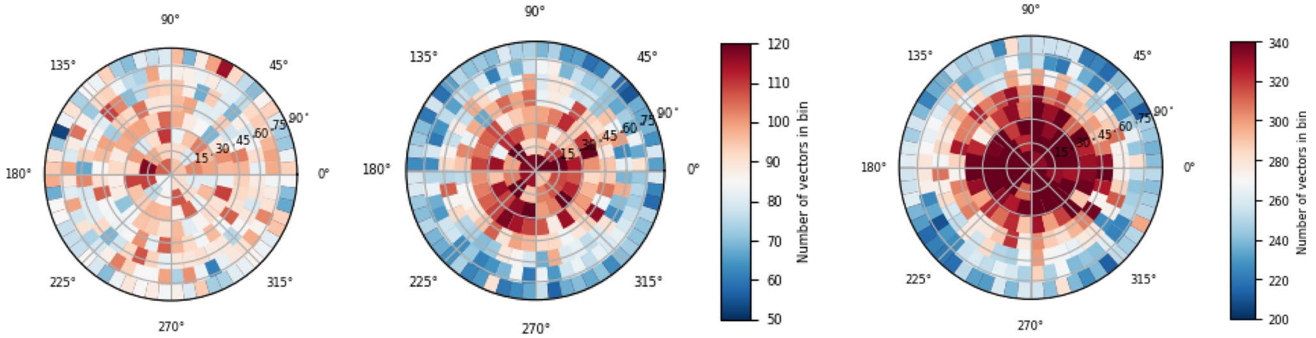

Fig. 14 Lambert azimuthal projection of binned contact normal orientations for the SiG specimen (left), SiS sand specimen (center), and W3 sand specimen (right)

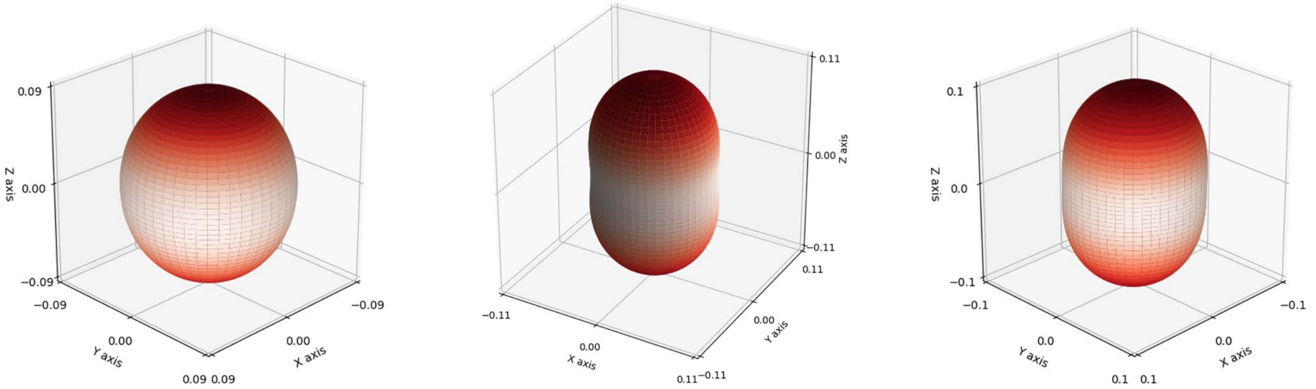

Fig. 15 Surface plots of the contact fabric tensors for the SiG specimen (left), SiS sand specimen (center), and W3 sand specimen (right)

Table 2 Coordination numbers *CN* and the contact fabric anisotropies *a* for the SiG, SiS, and W3 specimens

Material	*CN* [−]	*a* [−]
SiG	7.17	0.14
SiS	7.12	0.56
W3	7.06	0.46

Lambert azimuthal equal area projection is used to visualise the three-dimensional contact normal orientations. In the case of several thousand orientations, these are binned when plotted, where the red colour represents a high density and the blue colour represents a low density of orientations. The orientations at the center of the projection are purely vertical, while those at the border are only horizontal. Orientations between these two extremes are distributed across all three directions (see also [31] for more information).

5.2 Interpretation of fabric

Figure 14 illustrates the Lambert azimuthal projection of binned contact normal orientations for the SiG mixture, as well as the sands SiS and W3, after their deposition under water. The surface plots of their contact fabric tensors are shown in Fig. 15. Furthermore, Table 2 contains the information on the coordination numbers and the contact fabric anisotropies for the SiG, SiS, and W3 specimens.

In natural SiS and W3 sands, most contact normals are oriented between 45 and 90 °, shown by the red bins in the central region of the Lambert azimuthal projection (Fig. 14). Therefore, most grains in these sands, after beeing deposited under water, are aligned with their longest axis within the horizontal plane and are inclined up to 45 °, which indicates a clear similarity in their contact fabric. However, the number of orientation vectors in the bins is significantly higher for W3 sand, reflecting the differences in the grain size distribution compared to the SiS sand.

The similarity of the contact fabric is additionally confirmed through the surface plots of the contact fabric tensors of these sands (Fig. 15). The SiS sand has a more anisotropic fabric since the surface plot of its contact fabric tensor is peanut-shaped, while it approaches a capsule in the case of the W3 sand. Furthermore, the coordination number and the scalar anisotropies (Table 2) of these sands are very similar and thus, support the previous observations. Since all sands from Sect. 4 were prepared with the same method, it can be expected that their fabrics are similar. Thus, it seems that the same fabric, in spite of the large differences in D_r, is responsible for the similar excess PWP build-up in different sands, as shown in Fig. 10.

The contact normal orientations of the SiG mixture are randomly distributed, as shown in Fig. 14 left. This can be attributed to the round shape of glass beads, where no preferred grain orientations can be identified. For a better comparison with the SiS sand, the same binning range was applied. Also, the sphere-like surface plot of the contact fabric tensor for the SiG mixture (Fig. 15 left) and the contact fabric anisotropy (Table 2) confirm the isotropic fabric of glass beads. Such, isotropic fabric, characterised by a great amount of contact normals in vertical as well as in horizontal direction, can offer a higher resistance to the horizontal shearing (compared to natural sands), which results in a very low C_l(Fig. 10).

Regarding the fast excess PWP build-up observed in Hostun sand (Fig. 10) and the corresponding high C_l value, a dynamic image analysis [32] was performed on a large number of its grains. The aspect ratio AR, defined as the ratio of the width to the height of individual particles, was determined to $AR = 0.672$, indicating highly elongated grains. In comparison, sands SiS and W3 have $AR = 0.752$ and $AR = 0.739$, respectively.

The elongated shape of Hostun sand grains suggests that the most grains align subhorizontally after their deposition under water. This grain arrangement creates a fabric where many contact normals are oriented subvertically, which results in a significantly less resistance to horizontal cyclic shear loading in the PWP Tester, compared to the fabrics of the remaining sands. Unfortunately, we were not able to perform also a μCT scan of the Hostun sand sedimented in water in order to confirm this hypothesis.

6 Conclusions

Relative density is often considered the key factor influencing the accumulation of the excess pore water pressure in coarse-grained soils during undrained shearing. While the importance of relative density is indisputable, the results suggest that the influence of soil fabric can be equally significant.

Tests with 41 different materials showed that the relative density after the soil deposition under water varies from loose to dense state. Additionally, materials with different granulometric characteristics, such as glass beads, clean sands, sands with fines, and crushed sands, can be clearly distinguished based on their relative density after the deposition under water and their void ratio range.

Each deposition method is likely to produce a specific type of soil fabric. However, standard index tests used to determine limit densities do not account for these different deposition fabrics. As a result, relative densities calculated based on these tests may not realistically reflect the true characteristics of the soil. Thus, a more suitable measure for describing soil state, when analysing the excess PWP build-up, is relative density calculated with the limit density accounting for the soil fabric created by the deposition method.

The newly developed PWP Tester enables a fast and simple testing of the excess PWP evolution in coarse-grained soils due to cyclic shear. The soil specimens are tested following a clearly defined procedure, which includes the soil deposition (sedimentation) under water, isotropic consolidation, and cyclic displacements at the top cap in the horizontal direction at undrained conditions. The parameter characterising the evolution of the excess PWP under a certain soil state and loading conditions is denoted as C_l and quantifies the rate of the excess PWP build-up.

Although the relative densities, as determined by standard tests, vary significantly among different soils after their sedimentation in water, the rate of the excess PWP evolution during undrained shearing remains comparable. However, the relative densities based on the minimum dry density, obtained from soil sedimentation in water, fall within a narrow range and can be considered more suitable for describing the soil state when analysing the build-up of the excess PWP in different soils. This conclusion is further supported by the analysis of soil fabric extracted from μCT images of two natural sands, which shows similarities in their fabric after deposition in water and is obviously responsible for the excess PWP accumulation. This emphasizes that a prediction of the excess PWP build-up, which can produce soil liquefaction after a sufficient number of cycles, is not reliable if based only on (conventional) relative densities at one particular effective stress.

Appendix A: Physical properties of tested materials

See Table 3.

Table 3 Physical properties of tested materials

Nr	Material	d_{50} [mm]	C_U [−]	*FC* [%]	ρ_s g/cm^3	$e_{\min}$ [−]	$e_{\max}$ [−]	$e^w_{\max}$ [−]	φ_c [°]
1	SiS	0.943	1.2	0.0	2.65	0.579	0.865	0.858	30.0
2	SiG	1.046	1.6	0.0	2.59	0.430	0.674	0.667	22.6
3	DDFS	1.267	1.5	0.0	2.63	0.614	0.916	0.929	34.4
4	DDS	0.521	3.7	0.2	2.65	0.471	0.840	0.667	30.9
5	CK	0.800	3.6	0.3	2.67	0.620	1.058	1.026	35.2
6	HS	0.338	1.6	0.2	2.65	0.583	1.064	1.035	33.4
7	TS	0.208	1.4	0.0	2.63	0.566	0.952	0.887	30.8
8	W1	0.436	1.9	0.5	2.64	0.494	0.844	0.775	32.5
9	W3	0.621	2.2	0.1	2.64	0.546	0.846	0.787	31.2
10	W4	0.754	2.7	0.6	2.63	0.428	0.760	0.659	31.4
11	W4G	0.714	3.0	0.0	2.50	0.297	0.504	0.485	21.1
12	W5	0.589	2.9	0.8	2.64	0.434	0.778	0.683	33.8
13	W6	0.120	1.5	0.5	2.65	0.674	1.105	0.952	32.2
14	W7	0.627	2.8	0.6	2.64	0.422	0.776	0.663	33.4
15	W8	0.647	3.0	0.6	2.64	0.404	0.767	0.646	32.2
16	W9	0.418	1.9	0.7	2.64	0.472	0.844	0.730	32.9
17	Kali1	0.477	4.4	6.8	2.64	0.407	0.893	0.647	35.2
18	Kali2	0.430	1.9	2.6	2.64	0.546	0.960	0.751	34.4
19	Kali3	0.840	4.3	3.1	2.64	0.336	0.909	0.611	33.7
20	BBGr	0.493	4.5	6.4	2.64	0.386	0.881	0.637	32.7
21	BBGe	0.434	1.9	2.5	2.63	0.461	0.910	0.767	32.1
22	NRW1	0.272	1.9	4.8	2.63	0.543	1.207	0.895	33.8
23	NRW2	0.430	2.0	3.1	2.64	0.546	1.009	0.795	33.3
24	OS	0.262	1.5	0.3	2.65	0.513	0.886	0.808	32.6
25	GS	0.283	1.8	0.0	2.65	0.447	0.766	0.669	30.2
26	HiS	0.314	3.4	2.3	2.65	0.443	0.781	0.724	34.6
27	L1G	0.112	1.6	1.6	2.48	0.524	0.696	0.685	25.2
28	L2G	0.202	1.6	0.0	2.47	0.518	0.690	0.685	24.3
29	L4G	0.687	2.0	0.0	2.50	0.505	0.665	0.682	23.8
30	L6G	2.010	1.6	0.0	2.56	0.516	0.659	0.688	23.2
31	L12G	0.500	2.8	0.0	2.51	0.405	0.563	0.567	25.2
32	L16G	0.469	7.0	0.1	2.51	0.285	0.415	0.455	25.3
33	L1C	0.113	1.6	0.0	2.65	0.747	1.264	1.130	33.3
34	L2C	0.202	1.6	0.2	2.65	0.709	1.187	1.144	32.2
35	L4C	0.581	1.8	0.0	2.65	0.663	1.086	1.090	32.5
36	L12C	0.497	2.7	0.2	2.65	0.585	1.027	0.970	32.4
37	L16C	0.642	8.4	0.3	2.65	0.404	0.804	0.707	34.2
38	H1	0.494	3.6	0.5	2.66	0.348	0.673	0.591	33.0
39	H2	0.140	2.3	8.1	2.66	0.563	1.095	0.882	32.1
40	H3	0.127	–	21.5	2.67	0.532	0.998	0.679	34.8
41	H4	0.538	4.5	1.4	2.65	0.356	0.811	0.566	32.6

Here, d_{50} is the mean grain diameter, C_U is the uniformity coefficient, *FC* is the fines content, ρ_s is the grain density, $e_{\min}$ and $e_{\max}$ are the minimum and maximum void ratios, respectively, $e^w_{\max}$ is the maximum void radio after sedimentation under water and φ_c is the critical friction angle.

Acknowledgements We express our sincere gratitude to Sarah Müller for her dedicated efforts in conducting the experiments with the PWP Tester and her valuable contributions to the data collection for this study. We also thank the Center for Information Services and High Performance Computing (ZIH) at TU Dresden for providing generous allocations of computational resources. Further acknowledgments go to Prof. Torsten Wichtmann for providing numerous materials for this study.

Author contributions Ivo Herle proposed the research presented here and highly contributed to the conception of this work. The data analysis, development of the PWP Tester, and analysis of the μCT images were predominantly carried out by Božana Baćić. Martin Oppermann contributed by acquiring the radiographs and reconstructing them into μCT images. The first draft of the manuscript was prepared by Božana Baćić and was critically reviewed and commented by Ivo Herle.

Funding Open Access funding enabled and organized by Projekt DEAL.
This research has been funded by the German Research Founda-

tion (DFG, Deutsche Forschungsgemeinschaft) - project number: 316451575.

Data availability The experimental data used in this article will be made available from the first author upon reasonable request.

Code availability The open source software *spam* [30] has been used for the analysis of the μCT images. Its documentation can be accessed here: https://www.spam-project.dev/docs/

Declarations

Conflict of interest The authors declare that they have no conflict of interest.

Ethics approval Not applicable.

Consent to participate Not applicable.

Consent for publication Not applicable.

References

1. Oda, M.: Initial fabrics and their relations to mechanical properties of granular material. Soils Found. **12**(1), 17–36 (1972). https://doi.org/10.3208/sandf1960.12.17
2. Oda, M., Konishi, J., Nemat-Nasser, S.: Some experimentally based fundamental results on the mechanical behaviour of granular materials. Géotechnique **30**(4), 479–495 (1980). https://doi.org/10.1680/geot.1980.30.4.479
3. Oda, M., Nemat-Nasser, S., Konishi, J.: Stress-induced anisotropy in granular masses. Soils Found. **25**(3), 85–97 (1985). https://doi.org/10.3208/sandf1972.25.3_85
4. Oda, M.: The mechanism of fabric changes during compressional deformation of sand. Soils Found. **12**(2), 1–18 (1972). https://doi.org/10.3208/sandf1972.12.1
5. Ochiai, H., Lade, P.V.: Three-dimensional behavior of sand with anisotropic fabric. J. Geotech. Eng. **109**(10), 1313–1328 (1983). https://doi.org/10.1061/(asce)0733-9410(1983)109:10(1313)
6. Miura, S., Toki, S.: Anisotropy in mechanical properties and its simulation of sands sampled from natural deposits. Soils Found. **24**(3), 69–84 (1984). https://doi.org/10.3208/sandf1972.24.3_69
7. Yang, Z.X., Li, X.S., Yang, J.: Quantifying and modelling fabric anisotropy of granular soils. Géotechnique **58**(4), 237–248 (2008). https://doi.org/10.1680/geot.2008.58.4.237
8. Sun, Q., Zheng, J., He, H., Li, Z.: Characterizing fabric anisotropy of air-pluviated sands. E3S Web Conf. **92**, 01003 (2019). https://doi.org/10.1051/e3sconf/20199201003
9. Ni, X., Ma, J., Sakaguchi, H., Zhang, F.: Fabric characteristics of in situ sand with/without liquefaction verified by anisotropy of magnetic susceptibility. J. Rock Mech. Geotech. Eng. **15**(5), 1274–1283 (2022). https://doi.org/10.1016/j.jrmge.2022.09.003
10. Oda, M., Koishikawa, I., Higuchi, T.: Experimental study of anisotropic shear strength of sand by plane strain test. Soils Found. **18**(1), 25–38 (1978). https://doi.org/10.3208/sandf1972.18.25
11. Ladd, R.: Preparing test specimens using undercompaction. Geotech. Test. J. **1**(1), 16 (1978). https://doi.org/10.1520/gtj10364j
12. Mulilis, J.P., Arulanandan, K., Mitchell, J.K., Chan, C.K., Seed, H.B.: Effects of sample preparation on sand liquefaction. J. Geotech. Geoenviron. Eng. **103**, 91–108 (1977). https://doi.org/10.1061/AJGEB6.0000387
13. Sze, H.Y., Yang, J.: Failure modes of sand in undrained cyclic loading: impact of sample preparation. J. Geotech. Geoenviron. Eng. **140**(1), 152–169 (2014). https://doi.org/10.1061/(ASCE)GT.1943-5606.0000971
14. Ishihara, K.: Liquefaction and flow failure during earthquakes. Géotechnique **43**(3), 351–451 (1993). https://doi.org/10.1680/geot.1993.43.3.351
15. Ishihara, K., Silver, M.L., Kitagawa, H.: Cyclic strength of undisturbed sands obtained by a piston sampler. Soils Found. **19**(3), 61–76 (1979)
16. Tatsuoka, F., Ochi, K., Fujii, S., Okamoto, M.: Cyclic undrained triaxial and torsional shear strength of sands for different sample preparation methods. Soils Found. **26**(3), 23–41 (1986). https://doi.org/10.3208/sandf1972.26.3_23
17. Nagase, H., Ishihara, K.: Effects of load irregularity on the cyclic behaviour of sand. Soil Dyn. Earthq. Eng. **6**(4), 239–249 (1987)
18. Hatanaka, M., Uchida, A., Oh-oka, H.: Correlation between the liquefaction strengths of saturated sands obtained by in-situ freezing method and rotary-type triple tube method. Soils Found. **35**(2), 67–75 (1995)
19. Oda, M., Kawamoto, K., Suzuki, K., Fujimori, H., Sato, M.: Microstructural interpretation on reliquefaction of saturated granular soils under cyclic loading. J. Geotech. Geoenviron. Eng. **127**(5), 416 (2001). https://doi.org/10.1061/(ASCE)1090-0241(2001)127:5(416)
20. Hatanaka, M., Feng, L., Matsumura, N., Yasu, H.: A study on the engineering properties of sand improved by the sand compaction pile method. Soils Found. **48**(1), 73–85 (2008)
21. Ahmadi, M.M., Akbari Paydar, N.: Requirements for soil-specific correlation between shear wave velocity and liquefaction resistance of sands. Soil Dyn. Earthq. Eng. **57**, 152–163 (2014)
22. Wichtmann, T., Triantafyllidis, T.: An experimental database for the development, calibration and verification of constitutive models for sand with focus to cyclic loading: part I— tests with monotonic loading and stress cycles. Acta Geotech. **11**(4), 739–761 (2015). https://doi.org/10.1007/s11440-015-0402-z
23. Seed, H.B., Idriss, I.M.: Simplified procedure for evaluating soil liquefaction potential. J. Soil Mech. Found. Div. **97**(9), 1249–1273 (1971). https://doi.org/10.1061/jsfeaq.0001662
24. Bacic, B., Herle, I.: A simple method for the determination of sensitivity to density changes in sand liquefaction. Open Geomech. **2**, 1–8 (2020). https://doi.org/10.5802/ogeo.6
25. Baćić, B., Herle, I.: Density-dependent pore water pressure evolution in a simplified cyclic shear test. Int. J. Geosynth. Ground Eng. **9**(4), 47 (2023). https://doi.org/10.1007/s40891-023-00469-4
26. Bacic, B., Herle, I.: Vereinfachter zyklischer scherversuch zum PWD-Aufbau in grobkörnigen Böden. Geotechnik **46**(4), 210 (2023). https://doi.org/10.1002/gete.202300004
27. Baćić, B.: PWP tester–a simplified cyclic shear test for pore water pressure evolution in granular soils. TU Dresden, Dresden (2024)

28. NABau: DIN 18126: Baugrund, Untersuchung Von Bodenproben–Bestimmung der Dichte Nichtbindiger Böden Bei Lockerster und Dichtester Lagerung. Beuth Verlag GmbH, Berlin (2022)
29. Cubrinovski, M., Ishihara, K.: Maximum and minimum void ratio characteristics of sands. Soils Found. **42**(6), 65–78 (2002)
30. ...Stamati, O., Andò, E., Roubin, E., Cailletaud, R., Wiebicke, M., Pinzon, G., Couture, C., Hurley, R., Caulk, R., Caillerie, D., Matsushima, T., Bésuelle, P., Bertoni, F., Arnaud, T., Laborin, A., Rorato, R., Sun, Y., Tengattini, A., Okubadejo, O., Colliat, J.-B., Saadatfar, M., Garcia, F., Papazoglou, C., Vego, I., Brisard, S., Dijkstra, J., Birmpilis, G.: spam: Software for practical analysis of materials. J. Open Source Softw. **5**(51), 2286 (2020). https://doi.org/10.21105/joss.02286
31. Wiebicke, M., Andò, E., Šmilauer, V., Herle, I., Viggiani, G.: A benchmark strategy for the experimental measurement of contact fabric. Granul. Matter **21**(3), 54 (2019). https://doi.org/10.1007/s10035-019-0902-x
32. BSI: ISO 13322-2: Particle Size Analysis. Image Analysis Methods: Part 2 Dynamic Image Analysis Methods. British Standards Institution, London (2020)